

1
2
3 ***Fouling study of Nanofiltration membranes for sugar***
4 ***control in grape must. Analysis of resistances and the***
5 ***role of osmotic pressure***
6
7
8

9
10 C. Salgado¹, F.J. Carmona², L. Palacio¹, A. Hernández¹, P. Prádanos¹

11
12 ¹Grupo de Superficies y Materiales Porosos (SMAP, UA-UVA-CSIC), Dpto. de Física Aplicada,
13 Facultad de Ciencias, Universidad de Valladolid, 47071 Valladolid, Spain.

14 ²Dpto. de Física Aplicada. Esc. Politécnica. Universidad de Extremadura, 10003. Cáceres,
15 Spain.

16
17 **Abstract**
18
19

20
21
22 Three membranes are analyzed attending to their retention, flux and
23 fouling when used to nanofiltrate sugars in red grape musts. With high
24 molecular weight compounds, fouling develops from initial pore blocking to final
25 cake deposition. A decrease of resistance appears due to a decrease of the
26 effective transmembrane pressure and cake compaction. The final effective
27 pore size corresponds to that of the compacted cake.
28
29
30
31
32
33
34

35
36 Attending to flux decay and sugar retention, two membranes, HL and
37 SR3, are appropriate to reduce the content of sugar of red must. Specifically
38 SR3 shows the best passage of sugar and less fouling.
39
40
41
42
43
44
45
46
47

48 Keywords: Must nanofiltration, Fouling, Osmotic pressure, Cake Compaction,
49 Pore size
50
51
52
53
54
55
56
57
58
59
60

1. Introduction.

Membrane technology has been increasingly used in the beverage industry. For example, it is considered as an alternative concentration method of grape must ^[1]. This plays an important role in the beverage and wine industry since it contributes to the preservation of must and the concentrate is a natural sweetener in wine production, and a vitamin- and aroma-rich drink.

If the molecular weight of sugars in must is taken into account, nanofiltration, NF, is the membrane process to be chosen to retain them. It has been successfully used to increase the sugar content of grape must (to increase the final alcohol degree) in wine production ^[2]. Using a two stage NF process of grape must, Versari et al. ^[2] obtained relatively high sugar retentions (7–97%). Moreover, in their work García-Martin et al. ^[3, 4] studied the sugar reduction in musts by a two stage nanofiltration process to obtain wines with a slight alcohol reduction.

One of the main difficulties of NF technology is membrane fouling. Fouling in general causes deterioration in permeate quality and quantity, and eventually leads to an unavoidable membrane replacement ^[5]. This is because the dominant fouling mechanism in NF processes is the formation of a layer (a “cake”) that can significantly degrade membrane performance ^[6]. The conventional cake filtration theory consists from a corpus developed by Ruth ^[7] and successive researchers ^[8-12]. This approach states that during filtration, the cake thickness increases with time. In most cases, it also becomes more compact and its resistance to fluid flow increases accordingly. The main features of the dynamic behavior of cake filtration are the variation of the cake thickness, the evolution of the cake structure, the specific cake resistance and the total filtrate for a specified set of operating conditions ^[13, 14].

Fouling mechanisms during membrane filtration processes (i.e. Micro, MF, and Ultrafiltration, UF) have been studied in deepness along the last century ^[15-20]. Subsequently, Schippers and Verdow ^[21] studied the mechanisms involved during the performance of Reverse osmosis, RO. More recently, Listiarini et al.

[5, 22] applied these mechanisms for the analysis of the fouling of NF membranes.

In our previous work [23], a method was proposed to allow studying individually the resistances and fouling mechanism generated by low and high molecular weight solutes, LMW and HMW respectively, in red grape must NF.

The aim of the present work is to analyze in deepness the fouling mechanism, osmotic pressure and resistances of different NF membranes during the filtration of commercial grape must. Moreover, the assessment of these results and their influence on the performance of the NF membranes will conduct to the selection of the most appropriate one for sugar control in grape must.

For this purpose, the methodology suggested in previous studies [23] was applied in order to analyze individually the influence of LMW and HMW compounds.

2. Theory.

2.1. Permeate flux decrease and retention model.

When the overall filtration process is taken into account, the flux through the membrane per unit of membrane area can be written in terms of the applied transmembrane (hydraulic) pressure, $\Delta p_{h,s}$, the osmotic pressure gradient, $\Delta \pi_s$, the viscosity of the solution that goes through the pores of the membrane, η_p , and the system resistance. This is the sum of the membrane resistance, R_m , and the terms that depend on the fouling caused by the LMW, R_{fLMW} , and the HMW, R_{fHMW} , solutes [24-27]. In this way the permeate flow, J_v , can be calculated as

$$J_v = \frac{\Delta p_{h,s} - \Delta \pi_s}{\eta_p (R_m + R_f)} = \frac{\Delta p_{h,s} - \Delta \pi_s}{\eta_p (R_m + R_{fLMW} + R_{fHMW})} \quad (1)$$

Since the concentration of ionic species (potassium, calcium, sodium and magnesium) is similar on both sides of the membrane and the concentration of organic acids is much lower than that of sugars^[23], the increase of osmotic pressure can be determined by taking only into account the contributions of glucose and fructose by means of the van't Hoff's law:

$$\Delta\pi_s = \sum_{i=1}^N \Delta\pi_{s,i} = \sum_{i=1}^N \frac{RT}{M_i} (C_{m,i} - C_{p,i}) \quad (2)$$

Here, M_i is the molar weight of the i -th component, N is the number of components contributing to the osmotic pressure drop through the membrane system (here $N=2$ and i is glucose and fructose), R the gas constant and T the temperature. $C_{m,i}$ and $C_{p,i}$ are the concentrations on the membrane system interfaces at the feed and permeate sides respectively.

Figure 1 depicts the different concentrations and osmotic pressures to be considered along the membrane system.

Figure 1

2.2. Fouling mechanisms.

Compared to the solute size, NF membranes are provided with pores of a very small size. Hence, fouling mechanisms where it is assumed that all the solute molecules plug a pore (complete blocking); or are deposited inside the pores (standard blocking) seem inappropriate. Rather, molecules could deposit on other previously settled on the membrane surface or directly plug a pore as assumed in the so called intermediate blocking. Therefore, for the synthetic solution nanofiltration, so as for the first steps of must nanofiltration, flux decay should be caused by the intermediate blocking mechanism according to^[19, 20]:

$$\ln J_v(t) = -\kappa_i \frac{V_p(t)}{A_m} + \ln J_{v,0} \quad (3)$$

where κ_i is the intermediate blocking kinetic constant in m^{-1} , V_p is the permeated volume in m^3 and A_m the membrane surface area in m^2 .

After saturation of the intermediate mechanism, a cake would eventually be built. According to this model the time evolution of the process will be given by:

$$\frac{t}{V_P(t)} = \frac{\kappa_c}{2} V_P(t) + \frac{1}{J_{v,0} A_m} \quad (4)$$

where the kinetic constant κ_c (in $\text{s} \cdot \text{m}^{-6}$) is twice the Modified Fouling Index^[21], MFI, that is defined as the slope of the plot of t/V_P versus V_P .

2.3. Pressure drops along the membrane system.

As mentioned, in cake filtration mechanisms such as grape juice filtration, the feed passes through two contributions to the overall resistance that are placed in series: that of the membrane and that of the layer formed due to the fouling (cake).

In the same way, the effective applied pressure drop, the hydraulic pressure applied and the osmotic pressure through the membrane system at any time should be the sum of the contributions in the membrane and the cake. Then:

$$\left. \begin{aligned} \Delta p_{\text{eff},s} &= \Delta p_{\text{eff},m} + \Delta p_{\text{eff},c} \\ \Delta p_{h,s} &= \Delta p_{h,m} + \Delta p_{h,c} \\ \Delta \pi_s &= \Delta \pi_m + \Delta \pi_c \end{aligned} \right\} \quad (5)$$

Where:

$$\left. \begin{aligned} \Delta p_{\text{eff},s} &= \Delta p_{h,s} - \Delta \pi_s \\ \Delta p_{\text{eff},m} &= \Delta p_{h,m} - \Delta \pi_m \\ \Delta p_{\text{eff},c} &= \Delta p_{h,c} - \Delta \pi_c \end{aligned} \right\} \quad (6)$$

Therefore, according to Eq. (1), each effective pressure can be calculated as

$$\Delta p_{\text{eff},k} = J_v \eta_P R_k \quad k=s, m \text{ or } c \quad (7)$$

Now we need to know $\Delta \pi_k$ to get $\Delta p_{h,k}$ or vice versa from data on the resistances.

According to Eq. (2) we can get $\Delta\pi_c$ once the concentration at the membrane-cake interface, $C_{m,i}$, is known. The other contributions to the total osmotic pressure drop are easily accessible as far as they refer to the feed-cake and the membrane-permeate interfaces. But, according to the definition of the true retention of the solutes, R_i (i.e. glucose and fructose)^[23]:

$$C_{m,i} = \frac{C_{p,i}}{1-R_i} \quad (8)$$

When these calculations are done for the synthetic solution $C_{m,i}$ is the concentration of glucose or fructose on the membrane active layer because no cake would appear. $C_{m,i}$ can be calculated with Eq. (8) if it is accepted that the membranes sugars true retention is equal to that evaluated for the synthetic solution filtration and that it behaves in the same way when the cake appears as when it is not present. Eq. (2) also allows us to evaluate both $\Delta\pi_m$ and $\Delta\pi_s$. Then, by Eqs. (6) and (7), $\Delta p_{h,k}$ can be calculated. Then all the terms of pressure drops along the membrane system could be evaluated by using Eqs. (5) and (6).

2.4. Specific cake resistance. Principles of cake filtration.

The cake sheet formed over the membrane consists in a thin layer of solid particles through which the permeate flows. The specific cake resistance represents the fouling resistance caused by the fouling layer on the membrane, R_f , normalized by the accumulated cake mass per unit of membrane area^[22], so

$$\alpha = \frac{R_f A_m}{m_c} \quad (9)$$

Thus, according to Eq. (1) for the cake:

$$\alpha = \frac{\Delta p_{eff,c} A_m}{\eta_p J_v m_c} \quad (10)$$

where m_c is the mass of the cake deposited on the membrane surface.

A material balance allows the correlation of m_c with the permeate volume V_P (volume collected up to time t). If C_b is the bulk concentration of foulants, the mass of the particles deposited onto the membrane can be correlated to the permeated volume as

$$m_c = \gamma V_p C_b \quad (11)$$

where γ is a particle deposition factor (less than unity) that accounts for the reduction of cake mass due to its partial removal induced by the crossflow conditions. This coefficient was first proposed, by Sioutopoulos et al.^[28], in order to extrapolate specific cake resistance calculations to cross flow conditions. Therefore Eq. (9) could be used to evaluate α if C_b is known, and Eq. (10) can be used to get $\Delta p_{eff,c}$.

In order to calculate C_b along the filtration process, the following assumptions must be made:

1. The global concentration of foulants is considered to be that of the total dry extract of must, C_{DE} , which includes all matter that is non-volatile. This concentration was defined and determined in accordance to the OIV methods^[29]. These procedures require weighting at a temperature of 70 °C under vacuum of 25 mmHg until measuring a constant weight.
2. All the HMW compounds are always retained by the membrane; therefore the mass of these particles in the retentate side, m_{HMW} , is considered to be constant during the process.
3. Only the variation of the concentrations of glucose and fructose in the retentate were taken into account since their concentration is so high that the variation of the other LMW is considered negligible.

In accordance to these ideas, the concentration of HMW can be obtained as

$$C_{HMW} = C_{DE} - C_{T,0} \quad (12)$$

where $C_{T,0}$ is the initial total sugar concentration (glucose and fructose).

Moreover

$$m_{HMW} = C_{HMW} V_0 \quad (13)$$

V_0 being the initial volume of must.

Finally, C_b can be evaluated, as a function of time, by

$$C_b(t) = \frac{m_{HMV} + m_{TR}(t)}{V_R(t)} \quad (14)$$

where $m_{TR}(t)$ is the total sugar content and $V_R(t)$ the volume of the retentate at the filtration time t . Then, by using Eqs. (11) and (7), Eq. (10) can be used to calculate α .

Another strategy could be used for the estimation of α . In effect, according to Eqs. (1), (4) and (10), κ_c (that can be determined from the flux kinetics according to

$$\kappa_c = \frac{\gamma \eta_p C_b \alpha}{A_m^2 \Delta p_{eff,s}} \quad (15)$$

where, $\Delta p_{eff,s}$ is known because $\Delta \pi_s$ can be evaluated by eq. (2).

2.5. Pore size evolution.

Apparent pore size can be used to study flux decay through the analysis of its evolution. In order to estimate pore size, the Donan Steric and Partitioning model was used, with the introduction of the applied pressure gradient term as has been previously described^[30]. In these terms, the retention coefficient that a NF membrane presents can be written as

$$R = 1 - \frac{K_c \phi}{1 - (1 - K_c \phi) e^{-Pe}} \quad (16)$$

In this expression, the steric partition coefficient is $\phi = (1 - r_i/r_p)^2$ if a cylindrical geometry is assumed for the pores, being r_i and r_p the i -th component and pore radii respectively. The dimensionless Peclet number is given by:

$$Pe = \frac{K_c J_v \left(\frac{\Delta x}{A_k} \right)}{K_d D_i} = \frac{K_c J_v \left(\frac{r_p^2}{8 L_p \bar{\eta}} \right)}{K_d D_i} \quad (17)$$

where L_p is the water permeability, $\bar{\eta}$ the viscosity inside the pore, and Δx and A_k are the thickness and porosity of the membrane respectively. K_c and K_d represent the hindrance factors for convection and diffusion, respectively. These were evaluated as proposed by Dechadilok and Deen^[31]:

$$K_d = \frac{1}{(1-\lambda)^2} \left[1 + \frac{9}{8} \lambda \ln \lambda - 1.56034 \lambda + 1.91521 \lambda^3 - 2.81903 \lambda^4 + 0.270788 \lambda^5 \dots \right] \quad (18)$$

$$K_c = \left(\frac{1 + 3.867 \lambda - 1.907 \lambda^2 - 0.834 \lambda^3}{1 + 1.867 \lambda - 0.741 \lambda^2} \right) \quad (19)$$

where $\lambda = r_i / r_p$.

For the viscosity inside the pore, the model proposed by Wesolowska et al.^[32] is adopted, leading to:

$$\bar{\eta} = \left[\frac{(1-y)^4}{\eta_p} + \frac{(4y - 6y^2 + 4y^3 - y^4)}{10\eta_p} \right]^{-1} \quad (20)$$

where $y = d/r_p$, and $d=0.28$ nm.

Through this set of relations, the retention coefficient, R , is a function of the pore radius, r_p . From a set of data of, J_V and R , the pore radius could be estimated as the free parameter in the best fit to Eq. (17). In this work, instead of using the whole data set to estimate a unique r_p average value, each pair of values (J_V , R) were used to calculate the corresponding r_p from Eq. (17). As the filtration process modify flux rate and retention coefficient along the process, r_p changes with time too.

3. Materials and methods.

3.1. Membranes and experimental set-up.

Three different nanofiltration flat sheet membranes were tested: NF270 from Dow – Filmtec (the flatsheets were kindly supplied by the manufacturer);

1
2
3 HL from GE Water & Process Technologies and KMS SR3 from Koch
4 Membrane systems. The main characteristics of them are shown in Table 1.
5
6
7

8
9
10
11
12
13
14
15
16
17
18
19
20
21
22
23
24
25
26
27
28
29
30
31
32
33
34
35
36
37
38
39
40
41
42
43
44
45
46
47
48
49
50
51
52
53
54
55
56
57
58
59
60

TABLE 1

The experimental set-up used in this study is described in sufficient detail elsewhere^[23] thus only a brief summary is provided here. All the experiments were performed in a batch unit without dilution with a stainless steel flat sheet crossflow module with a single channel of length $L=110$ mm; height $H=0.5$ mm and width $W=60$ mm. These dimensions provide a membrane surface area $A_m=6.6 \cdot 10^{-3}$ m².

The operating conditions for every filtration processes were: feed temperature of 20°C, applied pressure of $35 \cdot 10^5$ Pa and retentate recirculation flow of 5 L/min. According to the dimensions of the channel, this supposes a feed tangential velocity on the membrane surface of 2.78 m/s.

3.2. Synthetic solution and commercial grape must.

Two NF processes were performed for each membrane. Firstly, a synthetic solution prepared in the laboratory containing the main low molecular weight compounds (LMW) of grape must was filtered. These are namely glucose (Glu), fructose (Fru), malic and tartaric acids, potassium, sodium, calcium and magnesium. The concentrations of this synthetic solution were the same that those reported in a previous work^[23]

Then it was carried out the filtration of commercial red must, which also contains high molecular weight compounds (HMW) such as polyphenols, polysaccharides and proteins. Attempting to reproduce the same conditions as in the first filtrate, the experiments with grape must were made using a brand new membrane flat sheet.

In this way, it was possible to analyze individually the influence of these HMW and LMW on the permeate flux decline, the true retention, the fouling mechanism and on the resistances to the permeate flux.

3.3. Experimental protocol.

The experimental protocol can be summarized as:

1. Membrane compaction was performed during one hour using Milli-Q water at $35 \cdot 10^5$ Pa, 20°C and a recirculation flow of 5 L/min, in order to avoid irreversible changes during operation. Under these conditions water permeability was determined. This measurement was repeated before and after all filtration and cleaning steps.
2. The membrane was soaked in the synthetic solution for 12 hours at 20-25°C. This was done to allow an initial deposition of foulants.
3. Nanofiltration of the synthetic solution of LMW at the operating conditions mentioned in 3.1.
4. Then, the membrane was cleaned with soft water at low pressure, under the same operating conditions of temperature and recirculation flow, during one hour sending both permeate and retentate to the drain. Afterwards it was rinsed with Milli-Q water using at least a volume equal to the system hold-up volume and sending the permeate and retentate to the drain too. Finally, the hydraulic permeability was measured.
5. Compaction and determination of hydraulic permeability of a new membrane sheet (step 1).
6. Soaking of the membrane in commercial red must during 12 hours with the same purpose as in step 2.
7. Nanofiltration of commercial red must at the operating conditions mentioned in 3.1.
8. A two stage membrane cleaning procedure consisting in a water rinse step followed by the use of a tensoactive solution of 0.1% sodium dodecyl sulfate as described in^[23]. After each step, hydraulic permeability was measured.

1
2
3 In each nanofiltration process, the permeate flux values were determined
4 by recording the time required to collect a known volume of filtrate (10 mL), first
5 every 15 minutes and when the flux reached more stable values, every 45
6 minutes. At the same time samples of permeate and retentate were taken in
7 order to determine their glucose and fructose content by liquid chromatography.
8
9

10
11 As mentioned, the filtration of both the synthetic solution and the red
12 must were carried out in a batch concentration mode. The permeate was sent to
13 the thermostated permeate vessel in order to collect it and the retentate was
14 recirculated to the thermostated feed vessel. The experiments were performed
15 until the permeate flux decreased to a more or less constant value for a
16 reasonable period of time (which depended on the membrane). The volumes
17 filtered were of the order of 2.5L of both, synthetic solution and red must.
18
19
20
21
22
23

24 25 26 **3.4. Deposition factor (γ)** 27

28
29
30 A significant issue is the extent to which the cross-flow operation may
31 affect the particle deposition on the membrane surface and therefore the
32 specific cake resistance. In the present investigation, a deposition factor γ was
33 estimated by determining the ratio of the true amount of must foulants deposited
34 on each membrane surface over the theoretical one.
35
36
37
38

39 The true mass deposition was determined by calculating the mass
40 difference between each fouled NF membrane and the respective new one. For
41 this purpose, red must filtrations were performed using the three membranes.
42
43
44

45 Pieces of both, fouled and clean, for each membrane were dried under
46 temperature (70°C) and pressure (25 mmHg) until measuring a constant weight
47 and the mass difference was measured. These conditions were established by
48 the OIV^[29] for grape and wine dry extract determination.
49
50
51

52 The theoretical cake mass was calculated by considering that all the dry
53 extract of must filtrated was attached to the cake layer on the basis of the total
54 permeate volume of each membrane test.
55
56
57

3.5. Analytical methods.

The chromatography system used for the identification and quantification of glucose and fructose was composed of a Shimadzu™ LC-9A HPLC apparatus, a Shimadzu™ Refractive Index device with a detector RID 6A, a Rheodyne™ injector with a 20 µL loop and the software Class-VP™. Separation was carried out isocratically in 100% deionized water at a flow rate of 0.5 mL/min at 85 °C using a Supelco™ ion exchange guard column and a Supelcogel™ Pb column.

3.6. SEM and AFM microscopy.

The surfaces of the membranes were imaged by Scanning Electron Microscopy, SEM. The samples were put on an aluminum plate and sheltered with a thin metal layer by a Polaron™ (SC7640 model) Sputter Coater. The electronic imaging device XL30 ES type EM (from Phillips™) was used and several accelerating voltages were applied to reach different magnifications.

Topography of the active layers was also studied through AFM. Images were acquired in the tapping mode at room temperature, with a Nanoscope IIIA microscope from Digital Instruments (of the Veeco™ Metrology Group). The tip was an Olympus™ OTESPA7 made out of an etched silicon probe aluminum coated with a length of 14 µm and an end with a radius of 7 nm. This allowed the minimization of the undesirable convolution of the tip shape and the membrane surface topography. Images were processed by means of the Nanoscope software version 5.30r3.sr3.

4. Results and discussion.

4.1. Permeate flux and permeability.

As mentioned, hydraulic permeability, L_P , was determined before and after every filtration or cleaning process and for each membrane as the slope of the J_V vs Δp plot with Milli-Q waterTM. From L_P data, the initial and final membrane resistances were calculated for $R_f=0$ and $\Delta\pi=0$. Results are shown in Table 2. It is clear that after the filtration and rinse of the synthetic solution, water permeability was slightly reduced for the three membranes. The main differences were detected after must nanofiltration and cleaning procedure. The SR3 membrane presented the highest permeability recovery (93%), followed by the HL membrane (70 %) and finally by NF270 (65 %). This means that SR3 has the most reversible fouling, presumably due to a less adhesion of molecules on the membrane surface or inside the pores.

TABLE 2

The permeate flux of the synthetic solution and red must filtrations for each membrane are plotted in Figure 2. In all cases, a decay of flux is observed. Here it can be noticed that the NF270 membrane has clearly the highest flux of the synthetic solution, followed by SR3 and HL. Bigger differences were appreciated mainly at the beginning of the red must NF, when the SR3 membrane presented the highest flux while NF270 and HL presented very similar fluxes, 3 times lower than that for the SR3. Besides, SR3 showed a less-sharp initial decline of flux (during around the initial 170 min = $10.2 \cdot 10^3$ s) followed by a very sharp flux decay. It is worth noting, that after a certain filtration time, the 3 membranes reached a more or less flat plateau around a quite similar low flux.

Figure 2

4.2. Sugars retention and passage.

1
2
3 True retentions of glucose and fructose have been evaluated. The
4 corresponding results are shown in Figure 3a (for the synthetic solution) and in
5 Figure 3b (for the commercial must) as a function of time.
6
7

8
9 **Figure 3**
10

11 Sugars retention remains practically constant during the synthetic
12 solution filtration for the three membranes. Both sugars (glucose and fructose)
13 were retained by all the membranes, especially by NF270 and SR3. NF270
14 presented the highest retention values (around 0.8) followed by HL (ranging
15 from 0.65 to 0.72) and finally by SR3 (between 0.44 and 0.52); which is in
16 accordance with the estimated radius for each of them, as we will show below.
17
18
19

20
21 These retentions do not agree with the nominal data shown in Table 1.
22 According to them, the SR3 membrane is the most retentive one for MgSO_4
23 while NF270 is the less retentive. This different salt rejection could be due to the
24 charge of the membranes and/or to their hydrophilicity. Given that the three
25 membranes have quite similar isoelectric points, around $\text{pH}=3.5^{[33-35]}$, the
26 difference must be mainly attributable to their contact angles. In fact, SR3 is the
27 most hydrophobic membrane (see Table 1)^[34, 36, 37], what should explain its high
28 retention of a charged and hydrated salt as MgSO_4 .
29
30
31
32
33
34

35 However, as it is shown in Figure 3b, the presence of HMW compounds
36 modifies the retention characteristics of the three membranes. The initial
37 retention falls drastically, between 0.2, for SR3 and 0.4 for NF270, keeping the
38 same order, as for the synthetic solution, for the three membranes. Subsequent
39 filtering leads to an increase in retention. This long time increase of retention
40 occurs equally for the three membranes, although much steeply for SR3; this
41 membrane and HL present values of R around 0.9, well above the value (0.8)
42 around which the NF270 finally stabilizes.
43
44
45
46
47
48

49 This evolution, when HMW compounds are present, must be attributed to
50 the formation and thickening of a gel layer on the membrane surface that acts
51 as a pseudo-membrane which lowers the passage of sugars through the
52 membrane by changing both: selectivity and permeability of the overall
53
54
55
56
57
58
59
60

1
2
3 membrane. As seen in Figure 3b, the influence of this pseudo-membrane on
4 the membrane retention is more significant in the case of SR3.
5
6
7

8 9 **4.3. Analysis of the fouling mechanisms.**

10
11
12
13 In order to analyze the fouling kinetics of both the synthetic solution and
14 the red must filtrations in a quantitative way, the previously outlined fouling
15 models ^[19, 20] have been used to fit the experimental data. The intermediate
16 blocking model seems to be compatible with data corresponding to the filtration
17 of the synthetic solutions and with the first steps of must filtration. The slopes of
18 the synthetic solution fits for the intermediate model, given by Eq. (3), were
19 similar for the three membranes. Note that, the slope is related with the area of
20 the membrane blocked per unit of total volume flown (through κ_f). The values for
21 κ_f are shown in Table 3. The highest κ_f was obtained for HL, followed by SR3
22 and finally by NF270.
23
24
25
26
27
28
29

30
31 TABLE 3

32
33 Figure 4a shows, as an example, the plots of flux versus the total volume
34 flown over time for the synthetic solution and red must filtration for SR3, fitted to
35 the intermediate blocking model where it can be seen that the slope is much
36 higher for the must than for the synthetic solution revealing a faster fouling
37 kinetics. This should be due to the additional pore blocking caused by the high
38 molecular weight compounds probably affecting the widest pores in the
39 membrane. The corresponding kinetic constants for the three membranes and
40 the synthetic solution are shown in Table 3.
41
42
43
44
45

46
47 In Figure 4b, the corresponding flux decay for the red must filtration is
48 shown for the three membranes studied. The kinetic constants are also shown
49 in Table 3. The fastest kinetics corresponds now to NF270 followed by HL and
50 finally by SR3 – the order of decreasing initial sugars retention (see Figures 3a
51 and 3b). What seems reasonable, because more retention would lead to more
52 deposition and consequently to faster flux decay. Note that κ_f for NF270 was the
53 lowest one (slowest kinetics) for the synthetic solution, while it is the highest
54
55
56
57
58
59
60

(fastest kinetics) when HMW components are present (red must filtration). This increase in κ_f for the NF270 should be due to a high affinity (chemical or electrostatic) of the membrane material to these high molecular weight components. Note too that the less blocked area (less κ_f) corresponds to SR3 when HMW compounds are present.

Figure 4

Eq. (4) corresponding to the “cake formation” mechanism is plotted in Figure 5. Here it is clearly seen that, for the three membranes, this mechanism is followed after the initial intermediate blocking during nanofiltration of must. In general, the three membranes suffer little pore blocking, especially SR3, where this mechanism seems to occur only during the first 30 mL of filtration. It is worth noting that in the three cases, the cake filtration mechanism seems to be divided into two steps: cake formation and cake formation with compaction. In any case both, the cake fouling steps, are faster for HL and the corresponding initial κ_c is relatively low for SR3 while the final κ_c is lower for NF270 (less compaction). The values of these kinetic constants are shown in Table 3.

Figure 5

4.4. Microscopy.

Figure 6 provides AFM pictures of an SR3 membrane before having been fouled (a) and afterwards (b). It seems clear that, after fouling, there is a quite compact thick cake layer that reduces extraordinarily the roughness.

Figure 6

In Figure 7, two SEM pictures of an HL membrane before and after fouling are showed. The two pictures correspond to a 20 μm in size. The picture after fouling shows a small square area that was imaged previously to the big one but also after fouling. It seems clear that the electron beam damaged the cake layer. The same procedure on the unfouled membrane didn't leave any similar trace.

Figure 7

4.5. Resistances to the permeate flux.

The resistances to J_V due to the presence of LMW, R_{fLMW} , and HMW, R_{fHMW} , were determined and analyzed individually. The values of R_{fLMW} for the synthetic solution were calculated according to Eqs. (2) and (4) with $R_{fHMW}=0$. The kinetics of R_{fLMW} for each membrane during the filtration of the synthetic solution filtration is shown in Figure 8a. In this case, NF270 presented the lowest values of resistance due to fouling, followed by HL and by SR3. This was to be expected because this order appeared also in retention as was shown in Figure 3a. Higher retentions lead to increasing viscosity and osmotic pressure that resulted in higher resistance to flux and also to faster fouling according to their corresponding κ_i in Table 3.

The correlation between R_{fLMW} and the total sugar concentration (glucose and fructose) on the membrane surfaces, C_{mT} is shown in Figure 8b. There, it can be seen that the correlation between R_{fLMW} and C_{mT} is practically linear, so it can be concluded that the resistance due to the accumulation of sugars on the membrane surface is proportional to their surface concentration. When C_{mT} is similar for the three membranes (shadowed zone in Figure 8b) the SR3 membrane has the lowest resistance due to low molecular weight compounds, R_{fLMW} .

Figure 8

In the case of red must filtrations, the values of R_{fLMW} were determined by the calculation of C_{mT} and the use of the correlation between R_{fLMW} and C_{mT} obtained for the synthetic solution. Replacing R_{fLMW} in Eqs. (2) and (4), the values of R_{fHMW} were determined for each membrane. Figure 9 shows the

1
2
3 evolution, with the permeated volume, of the individual resistances due to
4 fouling (R_{fLMW} and R_{fHMW}) and their sum (R_f) for the three membranes. The
5 figure shows that during most of the nanofiltration process there is no significant
6 increase of R_{fLMW} as was also the case for the synthetic solution. When filtering
7 red musts, R_{fLMW} remains practically constant in comparison to R_{fHMW} which
8 increases progressively until reaching a maximum beyond which there is a
9 gradual small decrease. This mechanism is clearly followed by SR3 (Figure 9c).
10 In all cases, R_{fHMW} has more influence on the J_V decrease, but this phenomenon
11 seems to be lower for the SR3 membrane (Figure 9d). It is interesting to relate
12 the cake fouling mechanism (Figure 5) with the resistances analysis (Figures 8
13 and 9). For the three membranes, the maximum R_f (or R_{fHMW}) agrees fairly well
14 with the beginning of the third fouling mechanism, where the cake starts to be
15 compacted.
16
17
18
19
20
21
22
23
24

25 Figure 9
26
27
28
29

30 The specific cake resistance, α (total resistance divided by the mass
31 deposited per unit membrane area) (see Eq. (9)), can help to somehow
32 normalize the resistance to permeate flux due to the fouling generated by all the
33 species present in red must (R_f). As mentioned in section (2.4), there are two
34 methods proposed for the estimation of the specific resistance. First, the
35 specific cake resistance was calculated using Eq. (15) with C_b evaluated by Eq.
36 (14). For this purpose the numeric derivative of (t/V_P) versus V_P (Figure 5) is
37 performed to get $\kappa_c/2$. In this calculation, all the cake formation mechanism (with
38 and without compaction) was included. This was considered appropriate to
39 describe the evolution of this parameter along the complete filtration. This
40 differs from the methodology applied by Listiarini et al.^[5, 22] where a linear
41 regression was performed including only the portion corresponding to the cake
42 filtration without compression. The deposition factor γ was estimated for each
43 membrane in order to take into account the incomplete foulant deposition giving
44 the values shown in Table 3. Note that γ follows the tendency of κ_c (second
45 step).
46
47
48
49
50
51
52
53
54
55
56
57
58
59
60

1
2
3 In Figure 10, the evolution of this theoretical specific cake resistance as a
4 function of the filtered volume is shown for each membrane. It is worth noting,
5 that this parameter shows also a maximum followed by a slight decrease. The
6 arrows correspond to the maximal values of R_f for each membrane, which are
7 near the zone of maxima for their specific cake resistance. As expected, the
8 highest α was shown by HL followed by NF270. SR3 presented the lowest
9 values during the first period of filtration (around 175 mL) afterwards the
10 resistance increases following the tendencies appearing in κ_c (see Figure 6).
11 The results obtained for the resistances (R_f and α) and even for the cake
12 formation mechanism for SR3 explain its different flux decline trend. The less
13 sharp flux decline during the beginning of red must nanofiltration is due to a
14 lower cake formation with a low resistance (R_f and α). But later, the progressive
15 formation and mainly the compaction of the cake cause a flux decay to values
16 close to those for the other two membranes.
17
18
19
20
21
22
23
24
25

26
27 Figure 10
28

29 The second method proposed is the estimation of the specific resistance
30 α by using Eq. (19) and the experimental data. In Figure 11, the experimental
31 total fouling resistance, in fact evaluated by using Eqs. (2) and (4), is compared
32 with that evaluated from the specific resistance α by using Eqs. (9) and (15), for
33 the SR3 membrane. It can be appreciated that the calculated R_f follows the
34 same trend as the experimental one. Note that around maximal resistances, the
35 fouling kinetics give values for the resistance which are close to those directly
36 obtained from the Hagen-Poiseuille equation. For shorter time filtrations, fouling
37 kinetics underestimates (while for longer filtration times it overestimates) the
38 total fouling resistance. This can be attributed to the fact that the fouling
39 kinetics predicts a low cake formation and for longer periods the cake mass is
40 over estimated. All in all, Figure 11 shows that the method proposed for the
41 estimation of α using the fouling kinetics is acceptable since it describes the
42 behavior of the experimental data specially in the period where the cake should
43 be completely formed (before its compaction).
44
45
46
47
48
49
50
51
52
53

54
55 Figure 11
56
57

4.6. Evolution of pore radii.

Pore radii were calculated as the value that minimizes the sum of squared residuals, $(R_{\text{cal}} - R_{\text{exp}})^2$ for each data set, following the theoretical model explained in section 2.5. The fitted dependence between R and J_V obtained for the synthetic solution is plotted in Figure 12a using grey curves. Evidently, it is worth noting that the model was elaborated for a membrane with a constant average pore size, r_p ; while it seems clear that in our case the effective mean pore size should change during the process of filtration due to the corresponding fouling process that includes pore blocking. Thus, the gray lines in Figure 12a correspond to the mean pore size of the membrane during the filtration process. The average deviation of the experimental results of retention from the theoretical retention curves in Figure 13a are evaluated and shown in Figure 13b as a (linear) function of the kinetic constant of pore blocking (intermediate model). This shows that pore blocking is clearly the main phenomenon determining the variations of the actual effective pore radius.

Figure 12

During the permeation of must, there is a continuous increase of retention while flow decreases slowly. The progressive increase of retention is so high that it seems inappropriate to assume a single pore size. In this case the model has been applied to each measurement and the pore radius obtained as a function of the permeated volume. In Figure 13, the effective pore radii evaluated from red must retention experiments are shown. It can be seen that there is a clear reduction of the effective pore size of the membrane (much slower, although a little larger, for the SR3 membrane). The mean pore radii for the synthetic solution are also shown here, for the sake of comparison, by horizontal lines. It is clearly observed that SR3 has the biggest pore radii, while the smallest ones appear in NF270. It can also be seen that the final pore radii for all the membranes are around 0.3 nm. This fact indicates that effective

1
2
3 radius is determined mainly by the cake formed on the membrane, more than
4 by the membrane itself.
5
6

7
8
9
10
11
12
13
14
15
16
17
18
19
20
21
22
23
24
25
26
27
28
29
30
31
32
33
34
35
36
37
38
39
40
41
42
43
44
45
46
47
48
49
50
51
52
53
54
55
56
57
58
59
60

Figure 13

In spite of the final convergence in equivalent pore radii, initial details do show differences between the membranes, especially between SR3 and the other two. Figure 13 shows a clear and pronounced drop of pore radii during the very first filtration moments for NF270 and HL. This happens as a consequence of the pore blocking explained in previous paragraphs. In contrast, for SR3, the pore radius does not show any significant initial decrease.

It appears clear that, for HL and NF270, pore blocking is the main factor determining the effective pore size with a final smooth additional reduction of pore size caused by the formation of the cake. The SR3 membrane is only slightly influenced by pore blocking with a final deep reduction due to the cake deposit and its compaction.

The arrows in Figure 13 correspond to the maximal resistances (Figure 8). Thus, it seems clear that maximal resistance occurs when the rhythm of decrease in pore size due to the cake formation starts to stabilize. This is especially apparent for the SR3 membrane.

4.7. Pressure drops.

Figure 14 shows the evolution of osmotic pressures and total effective pressures through: the global membrane system, the whole membrane and the cake itself.

Referring to the osmotic pressure (figure 14a), it increases for the cake and the global membrane system (that seems to be controlled by the cake) and decreases for the membrane itself with time (permeated volume). Note that the maximum rate of change for all the osmotic pressure terms appear when the fouling resistance R_f has its maximum. Note that, in this case below, this maximum there are negative osmotic pressures for the cake what means that

1
2
3 concentration is higher at the cake-membrane interface than at the feed-cake
4 interface. After the maximum in resistance, all the interfaces from retentate to
5 permeate correspond to decreases in concentration.
6
7

8 It seems clear (see Figure 14b) that the effective pressure drop through
9 all the components of the membrane system and through the global system
10 decrease with time (permeated volume) and that the maximal fouling resistance
11 appears when these pressure drops decrease faster. It seems also clear that
12 most of the effective pressure drop happens through the cake.
13
14
15

16 It can be concluded that, in our case, the maximum in the fouling
17 resistance and the appearance of a change in cake kinetics appear when the
18 osmotic pressures acts reducing substantially and quickly the effective
19 pressure. Regarding to the passage from negative to positive osmotic pressures
20 for the cake this would happen when the cake is completely build due to
21 compression followed by a gradual (slower) compaction with an increase of the
22 concentration at the feed-cake interface.
23
24
25
26
27
28

29 Note that, for the three membranes, when the osmotic pressure of the
30 system starts to increase, sugars are retained at their maxima by the membrane
31 system, as can be seen in Figure 3b. The highest R_{fHMW} , R_{fLMW} and R_f
32 correspond to the beginning of the high retention plateau. This is especially
33 clear for the SR3 membrane. So, as already mentioned, the sugar retention
34 increase can be attributed to the formation of a cake layer on the membrane
35 surface but its compression (and the corresponding osmotic pressure increase
36 through the cake and subsequently through the membrane system) may be the
37 cause of the significant retention increase that stops increasing when cake is
38 completely built.
39
40
41
42
43
44
45

46
47 Figure 14
48

49 50 51 **5. Conclusions** 52

53
54
55 We have systematically studied the fouling mechanism and resistances and
56 their influence on the performance of three different NF membranes proposed
57
58

1
2
3 for sugar control of grape must. Moreover, a method was proposed for the
4 analysis of the different osmotic pressure gradients through the resistances of
5 the membrane system.
6
7

8 The fouling kinetics when high molecular weight compounds are present
9 consists in three consecutive steps: An initial pore blocking step followed by a
10 cake deposition phase and an increase in compression until arriving to
11 compaction giving a slower kinetics. When the cake is completely well
12 assembled, the sugar retention has arrived to the maximum and osmotic
13 pressure of the system increases as to reduce the effective pressure. This later
14 causes a decrease of cake resistance that was increasing until this moment.
15 The evolution of retention and the effective pore size reveals the convergence
16 of the effective pore size to that of the cake after compaction.
17
18
19
20
21
22

23
24 Moreover, when the cake is completely built, its compaction promotes an
25 increase of the concentration at the feed-cake interface causing a passage from
26 negative to positive osmotic pressures for the cake.
27
28

29 The analysis of the flux decay and retention of sugar in musts shows
30 that, two of the three membranes studied, HL and SR3 are appropriate to
31 reduce the content of sugar of red must. Specifically SR3 shows the best
32 passage of sugar and less fouling.
33
34
35
36
37
38

39 **6. Acknowledgements**

40 Authors would like to thank the “Ministerio de Ciencia e Innovación
41 (MCINN)” for the financial support of this work within the frame of the “Plan
42 Nacional de I+D+I” through the research projects CTQ2012-31076 and
43 MAT2011-25513. Also the Spanish “Junta de Castilla y Leon” has contributed
44 through the project VA248U13.
45
46
47
48

49
50 C. Salgado wants to thank the Spanish Ministry of Education for the grant
51 they gave to her within the frame of the “Plan Nacional de
52 Investigación Científica, Desarrollo e Innovación Tecnológica 2008-2011” (FPU
53 grant: AP2010-5769) to complete her PhD.
54
55
56
57
58
59
60

1
2
3 Authors acknowledge Dow-Filmtec for the free supply of membrane
4 flatsheet samples to conduct this research.
5
6
7

8
9 **Nomenclature**

10
11
12
13 **Roman**

14		
15	A_m	Membrane surface area (m^2)
16		
17	A_k	Membrane porosity
18		
19	$C_{0,i}$	Feed concentration of the i-th component ($kg\ m^{-3}$)
20		
21	C_b	Bulk concentration of foulants ($kg\ m^{-3}$)
22		
23	$C_{f,i}$	Feed concentration of the i-th component ($kg\ m^{-3}$)
24		
25	C_{DE}	Total dry extract of must ($kg\ m^{-3}$)
26		
27	C_{HMW}	Concentration of HMW ($kg\ m^{-3}$)
28		
29	$C_{m,i}$	Concentration of the i-th component on the bulk-cake interface
30		(membrane active layer) ($kg\ m^{-3}$)
31		
32	$C'_{m,i}$	Concentration of the i-th component on the membrane-cake
33		interface ($kg\ m^{-3}$)
34		
35	C_{mT}	Total sugar concentration on the membrane active layer ($kg\ m^{-3}$)
36		
37	$C_{p,i}$	Permeate concentration of the i-th component ($kg\ m^{-3}$)
38		
39	$C_{T,0}$	Initial total sugar concentration (glucose and fructose) of red must
40		($kg\ m^{-3}$)
41		
42	D_i	Diffusion coefficient of the i-th component ($m^2\ s^{-1}$)
43		
44	HMW	High molecular weight compounds
45		
46	J_v	Permeate flux per unit of area through the membrane ($m^3\ m^{-2}\ s^{-1}$)
47		
48	$J_{v,0}$	Permeate flux per unit of area through the membrane at time $t = 0$
49		($m^3\ m^{-2}\ s^{-1}$)
50		
51	K_c	Hindrance factor for convection given by Eq. (25)
52		
53		
54		
55		
56		
57		
58		
59		
60		

1		
2		
3	K_d	Hindrance factor for diffusion given by Eq. (26)
4		
5	$K_{m,i}$	Mass transfer coefficient of the i-th component at semipermeable
6		membranes (m s^{-1})
7		
8		
9	LMW	Low molecular weight compounds
10		
11	L_p	Water permeability ($\text{m Pa}^{-1} \text{s}^{-1}$)
12		
13	m_c	Mass of cake deposited on the membrane surface in (kg)
14		
15	m_{HMW}	Mass of HMW in the retentate (kg)
16		
17	M_i	Molar weight of the i-th component (kg mol^{-1})
18		
19	$m_{TR}(t)$	Total sugar content of the retentate at the filtration time t (kg)
20		
21	Pe	Peclet number
22		
23		
24	R	ideal gas constant ($1.987 \cdot 10^{-3} \text{ kcal mol}^{-1} \text{ K}^{-1}$)
25		
26	R_{fHMW}	Resistance due to fouling by high molecular weight compounds
27		(m^{-1})
28		
29		
30	R_{fLMW}	Resistance due to fouling by low molecular weight compounds
31		(m^{-1})
32		
33		
34	R_{fj}	General resistance due to fouling (m^{-1})
35		
36	R_f	Total resistance due to fouling (m^{-1})
37		
38	R_i	Membranes true retention for the i-th component
39		
40	R_m	Membrane resistance (m^{-1})
41		
42		
43	r_p	Pore radii (nm)
44		
45	r_i	Radii of the i-th component (nm)
46		
47	T	Absolute temperature (K)
48		
49	t	Filtration time
50		
51	V_0	Initial volume of grape must (m^3)
52		
53	V_p	Permeate volume (m^3)
54		
55	$V_R(t)$	Volume of the retentate at the filtration time t (m^3)
56		
57		
58		
59		
60		

Greek

α	Specific cake resistance (m kg^{-1})
γ	Deposition factor on the membrane surface
$\Delta p_{h,s}$	Applied transmembrane pressure (Pa)
$\Delta p_{eff,c}$	Effective pressure drop across the cake (Pa)
$\Delta p_{eff,m}$	Effective pressure drop across the membrane (Pa)
$\Delta p_{eff,s}$	Effective pressure drop across the system (Pa)
$\Delta p_{h,c}$	Hydraulic Pressure drop across the cake (Pa)
$\Delta p_{h,m}$	Hydraulic Pressure drop across the membrane (Pa)
Δx	Membrane thickness (m)
$\Delta \pi_c$	Osmotic pressure gradient across the cake-active layer interface (Pa)
$\Delta \pi_m$	Osmotic pressure gradient across the membrane-cake interface (Pa)
$\Delta \pi_s$	Osmotic pressure gradient across the membrane system (Pa)
η_p	Viscosity inside the membrane pore (Pa s)
κ_c	Kinetic constant for the cake model (s m^{-6})
κ_i	Kinetic constant for the intermediate blocking model (m^{-1})
λ	Ratio r_i/r_p
ϕ	Steric partition coefficient

References

- (1) Kiss, I.; Vatai, G.; Bekassy-Molnar, E., Must concentrate using membrane technology. *Desalination* **2004**, *162*, (0), 295-300.

- 1
2
3 (2) Versari, A.; Ferrarini, R.; Parpinello, G.P.; Galassi, S., Concentration of Grape
4 Must by Nanofiltration Membranes. *Food and Bioproducts Processing* **2003**, *81*, (3),
5 275-278.
6
7
8
9 (3) García-Martín, N.; Perez-Magariño, S.; Ortega-Heras, M.; González-Huerta, C.;
10 Mihnea, M.; González-Sanjosé, M.L.; Palacio, L.; Prádanos, P.; Hernández, A., Sugar
11 reduction in musts with nanofiltration membranes to obtain low alcohol-content
12 wines. *Separation and Purification Technology* **2010**, *76*, (2), 158-170
13
14
15
16 (4) Garcia-Martin, N.; Perez-Magarino, S.; Ortega-Heras, M.; Gonzalez-Huerta, C.;
17 Mihnea, M.; Gonzalez-Sanjose, M.L.; Palacio, L.; Pradanos, P.; Hernandez, A., Sugar
18 reduction in white and red musts with nanofiltration membranes. *Desalination and*
19 *water treatment* **2011**, *27*, (1-3), 167-174.
20
21
22
23
24 (5) Listiarini, K.; Chun, W.; Sun, D.D.; Leckie, J.O., Fouling mechanism and
25 resistance analyses of systems containing sodium alginate, calcium, alum and their
26 combination in dead-end fouling of nanofiltration membranes. *Journal of Membrane*
27 *Science* **2009**, *344*, (1–2), 244-251.
28
29
30
31 (6) Sioutopoulos, D.C.; Karabelas, A.J.; Yiantsios, S.G., Organic fouling of RO
32 membranes: Investigating the correlation of RO and UF fouling resistances for
33 predictive purposes. *Desalination* **2010**, *261*, (3), 272-283
34
35
36
37 (7) Ruth, B.F., Studies in Filtration III. Derivation of General Filtration Equations.
38 *Industrial & Engineering Chemistry* **1935**, *27*, (6), 708-723
39
40
41 (8) M J Matteson, C.O., *Filtration: Principles and Practices, Second Edition, Revised*
42 *and Expanded*; Editor Ed.^Eds.;Marcel Dekker: New York, 1987.
43
44
45 (9) Tiller, F.M., The role of porosity in filtration part 3: Variable-pressure—variable-
46 rate filtration. *AIChE Journal* **1958**, *4*, (2), 170-174
47
48
49 (10) Tiller, F.M., The role of porosity in filtration. Numerical methods for constant
50 rate and constant pressure filtration based on Kozeny's law. *Chem. Eng. Prog.* **1953**, *49*,
51 (9), 467-479.
52
53
54
55 (11) Tiller, F.M., The role of porosity in filtration. Part 2. Analytical equations for
56 constant rate filtration. *Chem. Eng. Prog.* **1955**, *51*, (6), 282-290.
57
58
59
60

- 1
2
3 (12) Tiller, F.M.; Cooper, H.R., The role of porosity in filtration: IV. Constant pressure
4 filtration. *AIChE J.* **1960**, *6*, (4), 595-601.
5
6
7 (13) Tien, C.; Bai, R., An assessment of the conventional cake filtration theory.
8 *Chemical Engineering Science* **2003**, *58*, (7), 1323-1336
9
10 (14) Vorobiev, E., Derivation of filtration equations incorporating the effect of
11 pressure redistribution on the cake–medium interface: A constant pressure filtration.
12 *Chemical Engineering Science* **2006**, *61*, (11), 3686-3697
13
14 (15) Hermans, P.H.; Bredee, H.L., Zur kenntnis der filtrationsgesetze. *Rec. Trav.*
15 *Chim.* **1935**, *54*, (9), 680-700.
16
17 (16) Gonsalves, V.E., A critical investigation on the viscose filtration process. *Recueil*
18 *des Travaux Chimiques des Pays-Bas* **1950**, *69*, (7), 873-903
19
20 (17) Grace, H.P., Structure and performance of filter media. I. The internal structure
21 of filter media. *AIChE Journal* **1956**, *2*, (3), 307-315
22
23 (18) Shirato, M.; Aragaki, T.; Iritani, E., Blocking filtration laws for filtration of power-
24 law non-Newtonian fluids. *J. Chem. Eng. Japan* **1979**, *12*, (2), 162-164.
25
26 (19) Bowen, W.R.; Calvo, J.I.; Hernández, A., Steps of membrane blocking in flux
27 decline during protein microfiltration. *Journal of Membrane Science* **1995**, *101*, (1–2),
28 153-165
29
30 (20) Herrero, C.; Prádanos, P.; Calvo, J.I.; Tejerina, F.; Hernández, A., Flux Decline in
31 Protein Microfiltration: Influence of Operative Parameters. *Journal of Colloid and*
32 *Interface Science* **1997**, *187*, (2), 344-351
33
34 (21) Schippers, J.C.; Verdouw, J., The modified fouling index, a method of
35 determining the fouling characteristics of water. *Desalination* **1980**, *32*, (0), 137-148.
36
37 (22) Listiarini, K.; Sun, D.D.; Leckie, J.O., Organic fouling of nanofiltration
38 membranes: Evaluating the effects of humic acid, calcium, alum coagulant and their
39 combinations on the specific cake resistance. *Journal of Membrane Science* **2009**, *332*,
40 (1–2), 56-62.
41
42
43
44
45
46
47
48
49
50
51
52
53
54
55
56
57
58
59
60

- 1
2
3 (23) Salgado, C.; Palacio, L.; Carmona, F.J.; Hernández, A.; Prádanos, P., Influence of
4 low and high molecular weight compounds on the permeate flux decline in
5 nanofiltration of red grape must. *Desalination* **2013**, *315*, 124-134
6
7
8
9 (24) Kozinski, A.A.; Lightfoot, E.N., Ultrafiltration of proteins in stagnation flow.
10 *AIChE Journal* **1971**, *17*, (1), 81-85.
11
12 (25) Goldsmith, R.L., Macromolecular Ultrafiltration with Microporous Membranes.
13 *Industrial & Engineering Chemistry Fundamentals* **1971**, *10*, (1), 113-120
14
15
16 (26) Jonsson, G., Boundary layer phenomena during ultrafiltration of dextran and
17 whey protein solutions. *Desalination* **1984**, *51*, (1), 61-77
18
19
20 (27) Wijmans, J.G.; Nakao, S.; Smolders, C.A., Flux limitation in ultrafiltration:
21 Osmotic pressure model and gel layer model. *Journal of Membrane Science* **1984**, *20*,
22 (2), 115-124
23
24
25 (28) Sioutopoulos, D.C.; Yiantsios, S.G.; Karabelas, A.J., Relation between fouling
26 characteristics of RO and UF membranes in experiments with colloidal organic and
27 inorganic species. *Journal of Membrane Science* **2010**, *350*, (1-2), 62-82
28
29
30 (29) OIV, *Compendium of International Methods of Wine and Must Analysis*; Editor
31 Ed.^Eds.;OIV: Paris, 2011.
32
33
34 (30) Silva, V.; Prádanos, P.; Palacio, L.; Calvo, J.I.; Hernández, A., Relevance of
35 hindrance factors and hydrodynamic pressure gradient in the modelization of the
36 transport of neutral solutes across nanofiltration membranes. *Chemical Engineering*
37 *Journal* **2009**, *149*, (1-3), 78-86
38
39
40 (31) Dechadilok, P.; Deen, W.M., Hindrance Factors for Diffusion and Convection in
41 Pores. *Industrial & Engineering Chemistry Research* **2006**, *45*, (21), 6953-6959
42
43
44 (32) Wesolowska, K.; Koter, S.; Bodzek, M., Modelling of nanofiltration in softening
45 water. *Desalination* **2004**, *162*, (0), 137-151.
46
47
48 (33) Oatley, D.L.; Llenas, L.; Pérez, R.; Williams, P.M.; Martínez-Lladó, X.; Rovira, M.,
49 Review of the dielectric properties of nanofiltration membranes and verification of the
50
51
52
53
54
55
56
57
58
59
60

1
2
3 single oriented layer approximation. *Advances in Colloid and Interface Science* **2012**,
4 173, 1-11.

5
6
7 (34) Rice, G.; Barber, A.R.; O'Connor, A.J.; Pihlajamaki, A.; Nystrom, M.; Stevens,
8 G.W.; Kentish, S.E., The influence of dairy salts on nanofiltration membrane charge.
9 *Journal of Food Engineering* **2011**, 107, (2), 164-172

10
11
12 (35) Al-Amoudi, A.; Williams, P.; Mandale, S.; Lovitt, R.W., Cleaning results of new
13 and fouled nanofiltration membrane characterized by zeta potential and permeability.
14 *Separation and Purification Technology* **2007**, 54, (2), 234-240.

15
16
17 (36) Mänttari, M.; Pekuri, T.; Nyström, M., NF270, a new membrane having
18 promising characteristics and being suitable for treatment of dilute effluents from the
19 paper industry. *Journal of Membrane Science* **2004**, 242, (1–2), 107-116

20
21
22 (37) Tang, C.Y.; Kwon, Y.-N.; Leckie, J.O., Effect of membrane chemistry and coating
23 layer on physiochemical properties of thin film composite polyamide RO and NF
24 membranes: II. Membrane physiochemical properties and their dependence on
25 polyamide and coating layers. *Desalination* **2009**, 242, (1–3), 168-182

26 27 28 **Figure captions**

29
30
31
32
33
34
35
36
37 Figure 1. Concentrations and osmotic pressures considered for the membrane
38 system. Here $\Delta\pi_c$ $\Delta\pi_m$ represent the osmotic pressure gradient across the
39 cake-active layer interface and across the membrane-cake interface
40 respectively; C_b = Bulk concentration of foulants; C_m Concentration on the
41 membrane active layer; C'_m Concentration on the membrane-cake interface;
42 and C_p Permeate concentration

43
44
45
46
47
48
49
50
51 Figure 2. Permeate flux time evolution of red must (RM) and synthetic solution
52 (SS) NF for each membrane.

1
2
3 Figure 3. Glucose (Glu) and fructose (Fru) retentions as a function of time: (a)
4 for the synthetic solution, (b) for red must ^[38]. Arrows correspond to maximum
5 total fouling resistances.
6
7

8
9
10 Figure 4.- $\ln(J_V)$ versus (V_p/A_m) : (a) The case of the SR3 membrane for the
11 synthetic solution (SS) and for the red must (RM), (b) The case of the three
12 membranes during red must NF as a comparison. Solid lines represent linear fit
13 to the intermediate blocking mechanism zone of the data, corresponding to Eq.
14
15
16
17
18
19 (3).
20

21
22 Figure 5.- (t/V_p) versus V_p for each membrane during red must NF. Open
23 symbols correspond to intermediate zone; filled symbols correspond to cake
24 formation mechanism zone.
25
26
27

28
29 Figure 6.- AFM pictures of the SR3 membrane before (a) and after (b) fouling.
30 Note that after fouling roughness has decreased substantially.
31
32

33
34 Figure 7.- SEM pictures of the HL membrane before (a) and after (b) fouling.
35 Note that after fouling a smaller square has been imaged and consequently the
36 deposited layer eroded by the electron beam.
37
38
39

40
41 Figure 8.- Evolution of R_{fLMW} for the synthetic solution for the three membranes:
42 (a) as a function of filtration time, (b) as a function of total sugar concentration in
43 the membrane surface $C_{m,T}$. Within the shadowed zone $C_{m,T}$ is similar for the
44 three membranes.
45
46
47
48
49

50
51 Figure 9.- Resistance due to fouling by low molecular weight, high molecular
52 weight, and all compounds (R_{fLMW} , R_{fHMW} and R_f respectively) in commercial red
53 must versus the total permeated volume for: (a) NF270, (b) HL and (c) SR3
54
55
56
57
58

1
2
3 membranes. (d) Comparison of the total fouling (R_f) resistance for the three
4
5 membranes. Arrows point to the respective maxima.
6
7

8 Figure 10.- Evolution of the specific cake resistance (α) as a function of the
9
10 permeate volume (V_p) for the three membranes during red must NF. Arrows
11
12 correspond to the maximum total fouling resistance for each membrane
13
14 (according to Figure 9d).
15
16

17 Figure 11.- Resistance due the total fouling (R_f) for the SR3 membrane. Black
18
19 triangles show the experimental resistance (see figure 9d) and white triangles
20
21 refer to the calculated ones.
22
23

24 Figure 12.- (a) Retention versus J_v for the synthetic solution filtration. Gray lines
25
26 are the fits using theoretical model for pore radius calculation (solid for Glucose,
27
28 dashed for fructose). Arrows indicate time line. (b) Mean deviation of the
29
30 experimental results on retention as a function of the kinetic constant of pore
31
32 blocking.
33
34
35

36 Figure 13.-Time evolution of pore radii calculated for each single data point of ●
37
38 NF270 (Glu), ■ HL (Glu), ▲ SR3 (Glu) of the red must NF process. Horizontal
39
40 lines represent the average values obtained for the synthetic solution NF along
41
42 the complete process. Arrows correspond to the maximum total fouling
43
44 resistance for each membrane (according to Figure 9d).
45
46
47

48 Figure 14.- Osmotic pressures (a) and effective total pressures (b) through the
49
50 membrane, cake and membrane system (membrane plus cake) for the SR3
51
52 membrane.
53
54
55

Tables**Table 1.** Main characteristics of the membranes.

Membrane	Manufacturer	MWCO (Da)	MgSO ₄ Rejection (%)	Operating range			Drop Contact angle (°)
				pH	P (10 ⁵ Pa)	T (°C)	
NF270	Dow	200 ^a – 400 ^b	97 ^{c,d}	3 – 10	< 41	< 45	30 ^g
HL	GE Water	150 – 300	98 ^{c,e}	3 – 10	< 40	< 50	27.5 ^h
SR3	Koch	200	99 ^{c,f}	4 - 10	< 44.8	< 50	49 ⁱ

^a[39], ^b[40], ^cAccording to the information provided by the manufacturers, ^dMgSO₄2000mg/L at 480 kPa, ^e MgSO₄ 2000mg/L at 690 kPa, ^f MgSO₄ 5000mg/L at 655 kPa, ^g[36], ^h[37], ⁱ[34].

Table 2. Hydraulic permeability and resistance of the membranes, initial value and after nanofiltration and cleaning processes.

Membrane	Water Permeability $L_p(10^{-11} \text{ m/Pa s})$				Membrane resistance $R_m(10^{13} \text{ m}^{-1})$			
	Before filtration	After synthetic solution rinse	After must rinse	After must cleaning with SDS	Before filtration	After synthetic solution rinse	After must rinse	After must cleaning with SDS
NF270	3.84	3.34	2.10	2.45	2.60	2.98	4.75	4.07
HL	3.70	3.35	2.21	2.56	2.69	2.98	4.52	3.90
KMS SR3	2.18	2.10	1.44	1.97	4.57	4.74	6.92	5.06

Table 3. Kinetic constants for fouling and the deposition factor γ .

Membrane	K_i (m ⁻¹)		κ_c (initial) (10 ¹¹ s m ⁻⁶)	κ_c (final) (10 ¹¹ s m ⁻⁶)	γ (10 ⁻³ dimensionless)
	SS global	RM initial	RM	RM	
SR3	8.61	88.17	1.60	8.92	1.30
HL	8.65	100.35	11.62	19.60	3.56
NF270	6.80	120.18	5.40	6.84	1.04

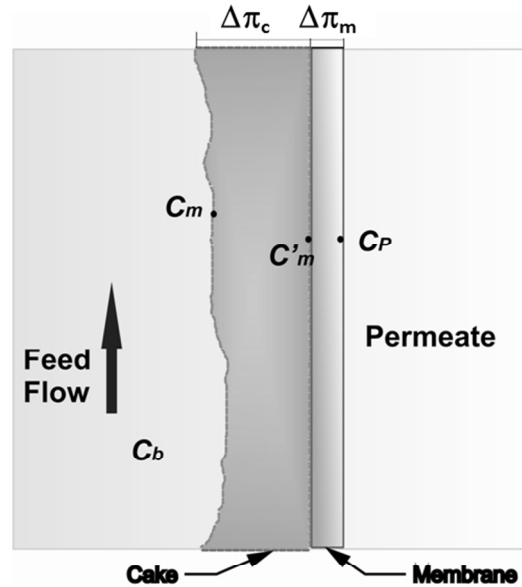


Figure 1. Concentrations and osmotic pressures considered for the membrane system. Here $\Delta\pi_c$ $\Delta\pi_m$ represent the osmotic pressure gradient across the cake-active layer interface and across the membrane-cake interface respectively; C_b = Bulk concentration of foulants; C_m Concentration on the membrane active layer; C'_m Concentration on the membrane-cake interface; and C_p Permeate concentration

254x190mm (96 x 96 DPI)

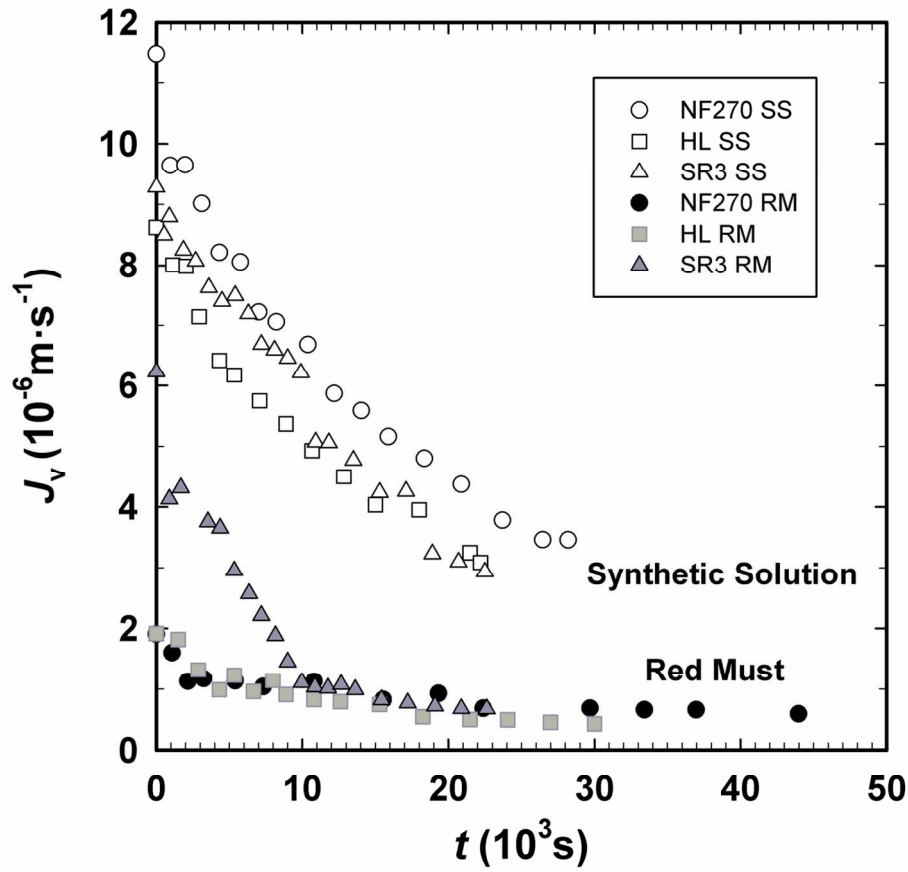


Figure 2. Permeate flux time evolution of red must (RM) and synthetic solution (SS) NF for each membrane. 124x113mm (300 x 300 DPI)

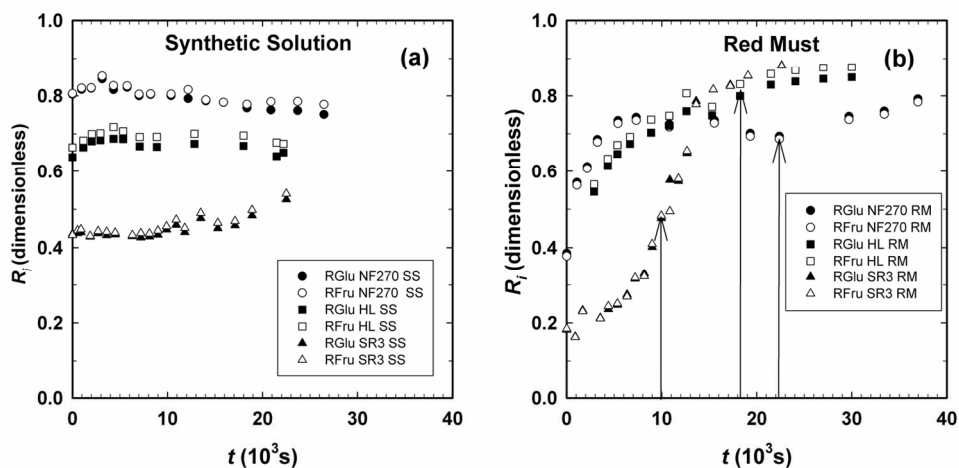


Figure 3. Glucose (Glu) and fructose (Fru) retentions as a function of time: (a) for the synthetic solution, (b) for red must [38]. Arrows correspond to maximum total fouling resistances.
134x68mm (300 x 300 DPI)

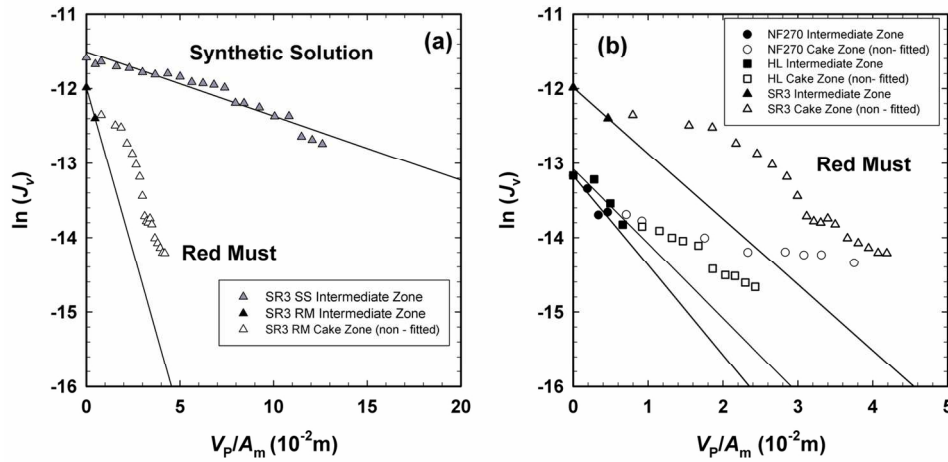


Figure 4. $\ln(J_v)$ versus (V_p/A_m) : (a) The case of the SR3 membrane for the synthetic solution (SS) and for the red must (RM), (b) The case of the three membranes during red must NF as a comparison. Solid lines represent linear fit to the intermediate blocking mechanism zone of the data, corresponding to Eq. (3).
137x70mm (300 x 300 DPI)

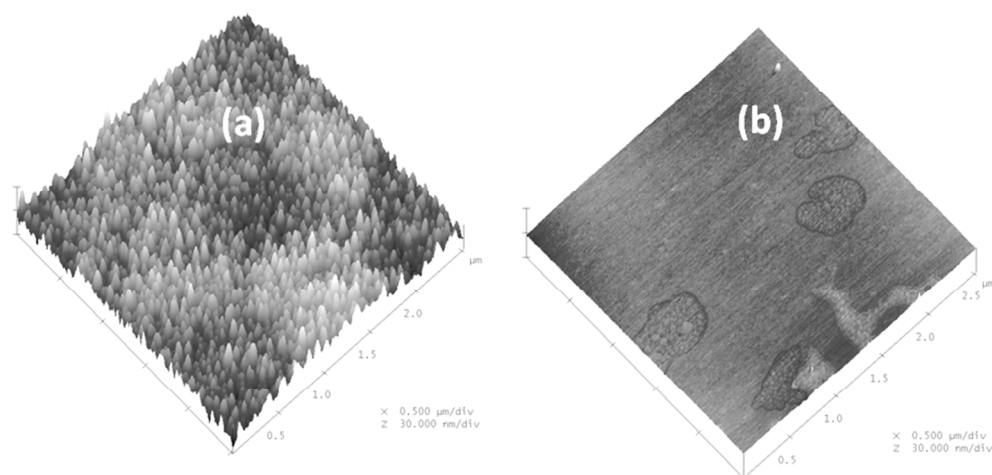


Figure 6. AFM pictures of the SR3 membrane before (a) and after (b) fouling. Note that after fouling roughness has decreased substantially.
243x120mm (96 x 96 DPI)

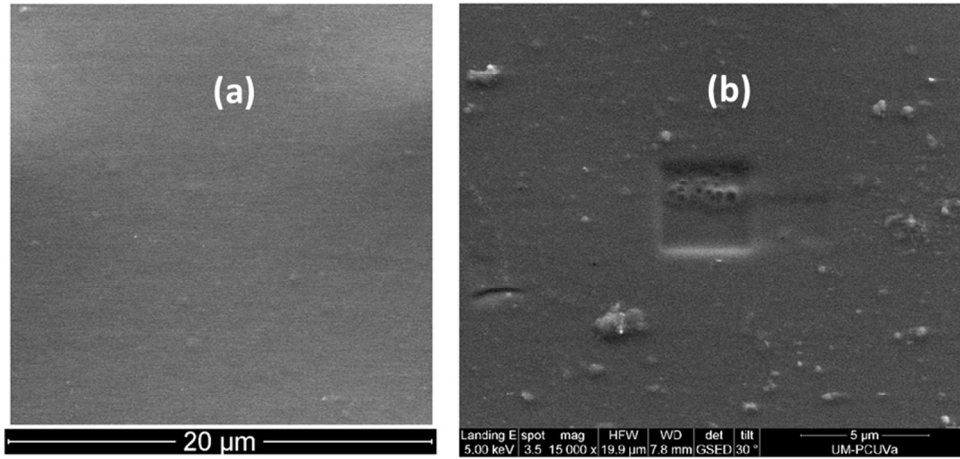


Figure 7. SEM pictures of the HL membrane before (a) and after (b) fouling. Note that after fouling a smaller square has been imaged and consequently the deposited layer eroded by the electron beam.
254x190mm (96 x 96 DPI)

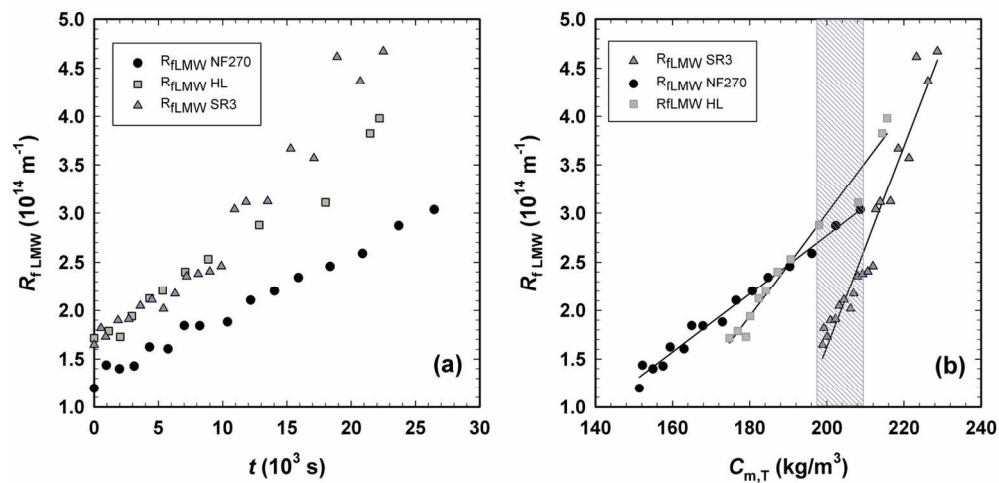


Figure 8. Evolution of $R_{f,LMW}$ for the synthetic solution for the three membranes: (a) as a function of filtration time, (b) as a function of total sugar concentration in the membrane surface $C_{m,T}$. Within the shaded zone $C_{m,T}$ is similar for the three membranes.

131x66mm (300 x 300 DPI)

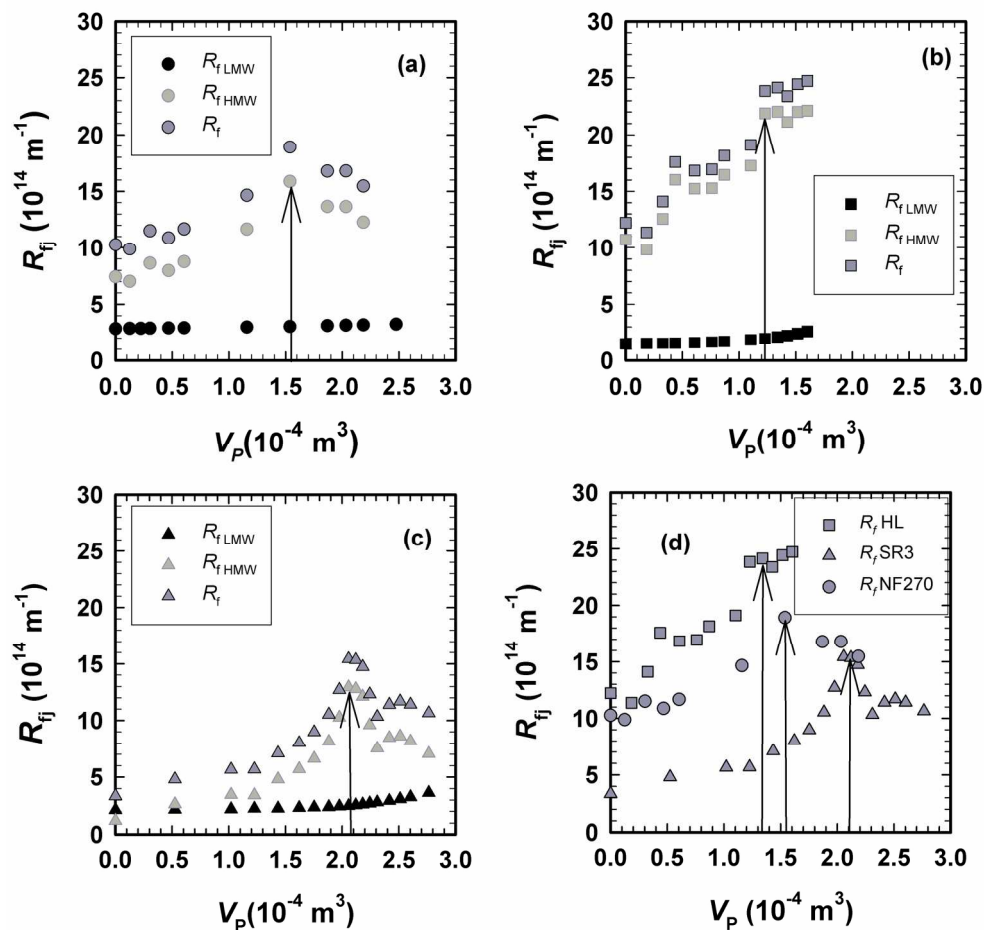


Figure 9. Resistance due to fouling by low molecular weight, high molecular weight, and all compounds ($R_{f,LMW}$, $R_{f,HMW}$ and R_f respectively) in commercial red must versus the total permeated volume for: (a) NF270, (b) HL and (c) SR3 membranes. (d) Comparison of the total fouling (R_f) resistance for the three membranes. Arrows point to the respective maxima.

177x177mm (300 x 300 DPI)

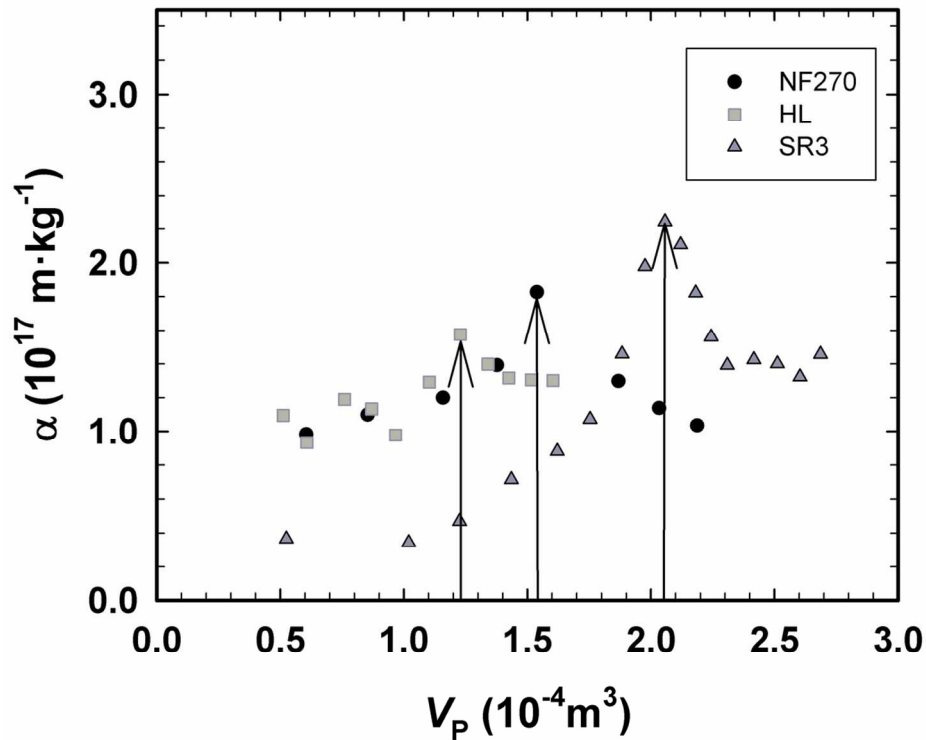


Figure 10. Evolution of the specific cake resistance (α) as a function of the permeate volume (V_p) for the three membranes during red must NF. Arrows correspond to the maximum total fouling resistance for each membrane (according to Figure 9d).
 115x97mm (300 x 300 DPI)

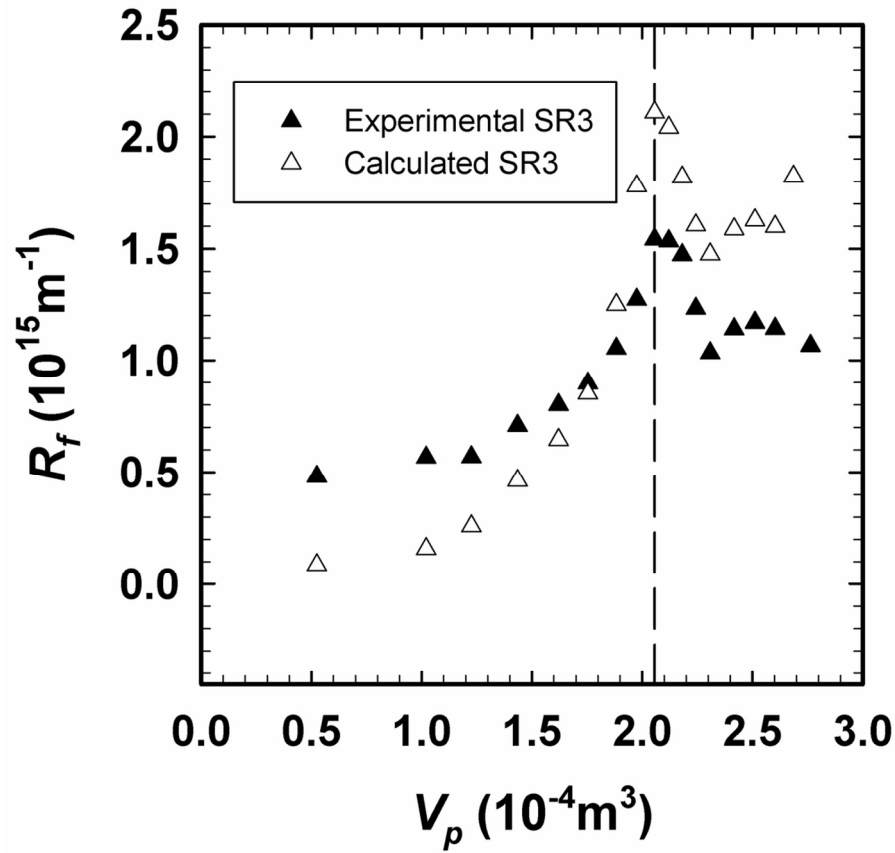


Figure 11. Resistance due the total fouling (R_f) for the SR3 membrane. Black triangles show the experimental resistance (see figure 9d) and white triangles refer to the calculated ones.
111x108mm (300 x 300 DPI)

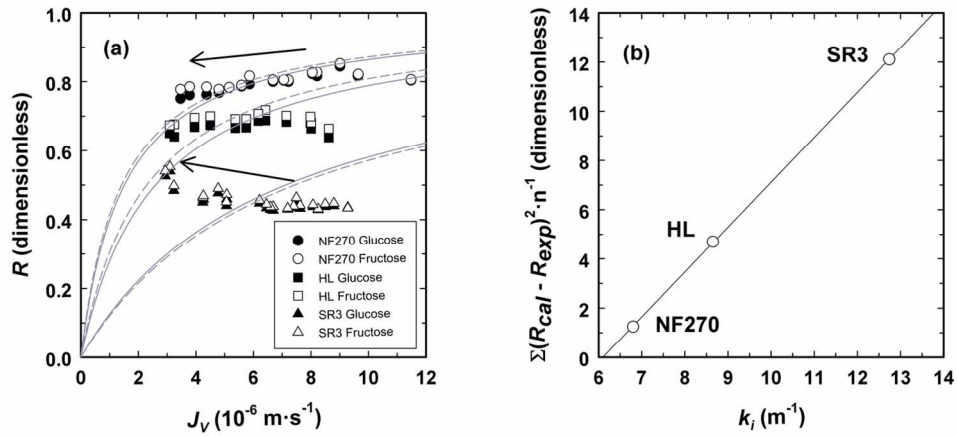


Figure 12. (a) Retention versus J_V for the synthetic solution filtration. Gray lines are the fits using theoretical model for pore radius calculation (solid for Glucose, dashed for fructose). Arrows indicate time line. (b) Mean deviation of the experimental results on retention as a function of the kinetic constant of pore blocking.

127x62mm (300 x 300 DPI)

Review Only

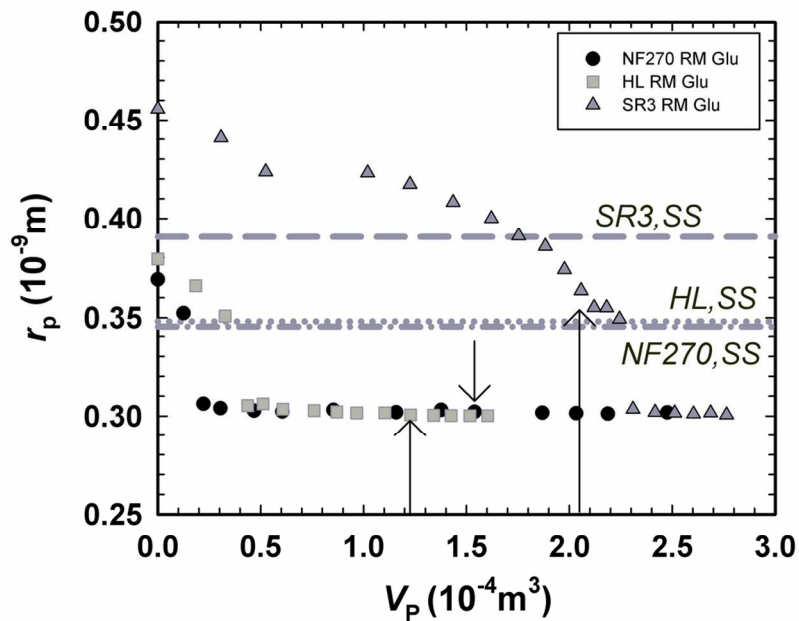


Figure 13. Time evolution of pore radii calculated for each single data point of \circ NF270 (Glu), \square HL (Glu), Δ SR3 (Glu) of the red must NF process. Horizontal lines represent the average values obtained for the synthetic solution NF along the complete process. Arrows correspond to the maximum total fouling resistance for each membrane (according to Figure 9d) $\bullet\bullet\bullet\blacksquare\Delta\Delta\square$ 115x82mm (300 x 300 DPI)

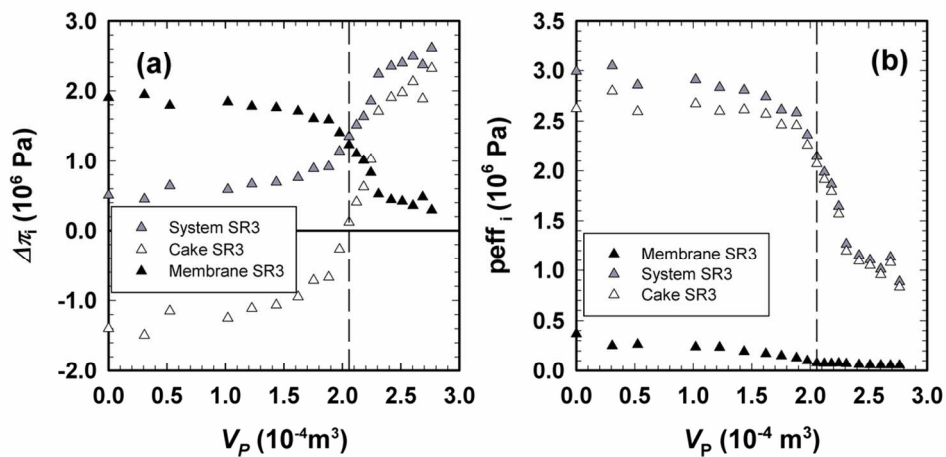


Figure 14. Osmotic pressures (a) and effective total pressures (b) through the membrane, cake and membrane system (membrane plus cake) for the SR3 membrane.
111x57mm (300 x 300 DPI)

Review Only